HYDROGEN CHLORIDE DETECTION IN ORION A ANI) MONOCEROS R2 AND I) ERIVATION OF THE $H^{35}Cl/H^{37}Cl$ ISO1OPIC RATIO.

M. Salez, M. A. Frerking, and W. D. Langer

Jet Propulsion Laboratory, California Institute of Technology

4800 Oak Grove Drive, Pasadena, CA 91109

ABSTRACT

We have detected the J= 1-0 transition of $H^{35}Cl$ in the Orion A and Monoceros R2 giant molecular clouds, using the Caltech Submillimeter Observatory and a new heterodyne receiver built at the Jet Propulsion Laboratory. We find a hydrogen chloride fractional abundance of a few 10^{-10}, and a depletion of gas-phase chlorine by a factor of 740 for Orion and 175 for Mon R2. For both sources, we derived the line optical depth and excitation temperature using the relative intensities of the hyperfine components and determined the abundance and excitation conditions with a large velocity gradient (LVG) model. The, LVG model indicates that radiative pumping of the molecules by moderately warm dust is required to explain the observed line intensities and optical depths, In addition, we report the first detection of the isotope $H^{37}Cl$ from its J=1-0 emission in Orion. Because the chemical reactions involving hydrogen chloride in molecular clouds are relatively simple, $[H^{35}Cl]/[H^{37}Cl]$ is believed to provide a good estimate of $[^{35}Cl]/[^{37}Cl]$. We find an isotopic ratio about 1.3 times that of the solar neighborhood, suggesting that enhancement occurs via a neutron enrichment process during the final stages of large mass stars' evolution.

Subject headings: ISM:molecules - ISM:abundances - ISM:individual: Orion, Mon R2

1. INTRODUCTION

The chemistry of chlorine and hydrogen chloride in interstellar molecular clouds has been investigated by several authors (Jura, 1974; Dalgarno et al, 1974; Blake, Anicich and Huntress, 1986). A major fraction of the gas-phase chlorine nuclei is believed to be in the form of HC1, produced from atomic chlorine according to the following set of reactions:

$$H_3^+ + Cl \rightarrow HCl^+ + H_2 \qquad (1)$$

$$HCl^+ + H_2 \rightarrow H_2Cl^+ + H \qquad (2)$$

$$H_2Cl^+ + e \rightarrow \begin{cases} HCl + H \\ Cl + H_2 \end{cases} \qquad (3)$$

$$H_2Cl^+ + CO \rightarrow HCl + HCO^+ \qquad (4)$$

The parent molecule H_2Cl^+ leads to HCl via electronic recombination(3) in the low-density clouds and by reaction with CO (4) in the denser clouds. HCl is mainly destroyed by photodissociation and reactions with C+ and H_3^+. In the dense molecular clouds characterized by little UV radiation and a low ionization rate, the HCl/Cl ratio is thus expected to be high. Early chemical models predicted a fractional abundance of HCl of a few 10^{-8}-10^{-7} (Dalgarno et al, 1974; Adams and Smith, 1985; Blake, Anicich and Huntress, 1986), making hydrogen chloride potentially one of the major coolants of molecular clouds due to its large J= 1-0 transition energy (Dalgarno, 1974; Goldsmith and Langer, 1978). However, Schilke, Phillips and Wang (1994) and Neufeld and Green (1994) have revisited the hydrogen chloride chemistry in molecular clouds taking into account additional reactions such as cosmic ray destruction, and derive. a much lower HC1 abundance, $X(HCl) < 210^{-9}$, and HCl/Cl no larger than 30%.

The first detection of the HCl J= 1-0 transition at 625.9 GHz was carried out from the Kuiper Airborne Observatory (KAO) by Blake, Keene and Phillips (1985, BKP hereafter) with an angular resolution of 2' and a spectral resolution of 1 km/s, using a hot-electron bolometer. Toward IRc2 in Orion A, BKP estimated $X(HCl) \simeq$ 5-5010-9. However, more recently, Schilke, Phillips and Wang (1994, SPW hereafter) have mapped the same region in HC1 J=1-0 with a

smaller angular resolution of 12" and better spectral resolution of 0.025 km/s from the Cal tech Submillimeter Observatory (CSO), and found smaller HCl fractional abundances of 4-1010-10. The solar system abundance of chlorine relative to H_2 is $3.7\,10^{-7}$ (Anders and Grevesse, 1989). Hence, assuming that HCl accounts for nearly 1/3 of the total chlorine, these observations imp] y a depletion factor of about 200 in Orion. Another observation of an astrophysical source in the ground-state transition of HCl was performed by Zmuidzinas et al. (1994) from the KAO. They detected hydrogen chloride in absorption toward Sagittarius B2. They derived $X(HCl) = 1.110\text{-}9$, which corresponds to a depletion factor of -110. Such high depiction is comparable to that of more refractory elements like Si and P, rather than those of C., N, and O, and seems to indicate that the remaining chlorine is condensed onto dust grains, as suggested from the work of Barlow and Silk (1 977), Harris, Gry and Bromage (1 984), and Joseph et al. (1 986) in more diffuse cloud structures.

The Orion molecular cloud (OMC-1) complex is a region of intense star formation, characterized by a predominance of very massive stars. Relatively nearby at 500 pc, this giant molecular cloud has been extensively studied at many wavelengths, Batrla et al, (1983) have mapped the cloud in the $NH_3(1,1)$ and (2,2) transitions, and studies of the dust continuum at $\lambda 1.3$ mm by Mezger et al. (1990) show the presence of 5-50 MO gas condensations, most of them self-luminous. The 'hard core' of OMC- 1 is a region of very high density ($n(H_2)>10^8\,cm^{-3}$) and high temperature (-100 K), powered by the infrared source 1Rc2 and a bipolar flow (Masson et al., 1984). Several clumps have been seen north and south of IRc2 in the CS J=2- 1 map made by Mundy et al (1 986). One of them, located 60" south of Orion KL, is 15"x25" in size with a hydrogen density larger than **5106** cm^{-3}. Mundy ct al. have derived a total mass of 10-50 MO for this clump, and the velocity dispersion is suggestive of in fall. This clump coincides with a local peak of HCl J=1 -O emission in the recent map of SPW (1994).

Monoceros R2 is another star formation region j n the general direction of the Orion complex but farther away, at 830 pc. Several authors (Montalban et al., 1990, Xie and Goldsmith,

1994, Tafalla, Bachiller and Wright, 1994) have mapped the large-scale structure of Mon R2 in CO and ^{13}CO, and have shown the molecular gas to be distributed in an 'eggplant-shaped' shell of radius 55' (13 pc), expanding at a velocity of 3,2 km/s. The dynamical time of this shell is 4 10^6 yr, similar to the age of the main sequence stars that power the reflection nebulae. The shell contains a total mass of 4 10^4 Mo, but is very inhomogeneous. The 22" large HII region (Dowries et al., 1975, Massi et al., 1985) associated with the infrared source IRS 1 and with a peak of 1300 μm emission (Walker et al., 1990), is believed (o be powered by the same source which triggers the CO outflow and heats the dust. The outflow NW-SE direction (Meyers-Rice and Lada, 1991) coincides with an elongated depression seen in the high resolution 9" HCO^+ map of Gonatas, Palmer and Novak (1 992), which suggests that HCO^+ traces the dense shocked regions collimating the outflow. The clumps of dense gas revealed by maps in several transitions of CS (Heyer et al., 1986, Wolf et al., 1990, Montalban et al., 1990, Tafalla, Bachiller and Wright, 1994) are clearly associated with peaks of dust continuum emission at 870 μm (Henning, Chini and Pfau, 1992) and with most infrared IRAS sources, suggestive of star formation within the shell. IRS 3 is an extended infrared source (Howard et al., 1994, Sellgren, Smith and Brooke, 1994), where evidence for a circumstellar disk is found from 0,5" resolution near-infrared observations (Koresko et al., 1993). It is associated with a CS clump containing about 8 MO, about **30"** west of the HII region,

2. OBSERVATIONS

As a result of the interaction between the electric field and the spin of the Cl nucleus, the J= 1 level of HCl is split into three h yperfine sublevels identified by their quantum number F"=1/2, 3/2, or 5/2. The J= 1-0 transition is thus the sum of three hyperfine transitions labeled F"-F'=3/2-3/2, 5/2-3/2, and I/2-3/2, whose corresponding frequencies are respective] y 625.9320, 625.9187, and 625.9016 GHz for $H^{35}Cl$ and 624.9883, 624.9778, and 624.9643 GHz for $H^{37}Cl$. This hyperfine structure allows the lines of the two isotopes to be identified with certainty.

The observations reported in this paper were made in late November 1993 with the Caltech Submillimeter Observatory (CSO) on Mauna Kea, Hawaii. The 10.4-m telescope has a diffraction-limited beam of 12" at 626 GHz. We have used the waveguide SIS heterodyne receiver newly fabricated at the Jet Propulsion Laboratory (Salez et al,, 1994), installed at the telescope's Cassegrain focus. The receiver noise temperature measured on the site was between 250 and 350 K double sideband (DSB). The noise temperature of the whole system, which includes the atmospheric attenuation near 626 GHz, was 2000 K - 3000 K DSB under the best weather conditions for large-elevation sources. The atmospheric conditions were routinely checked by monitoring the optical depth at zenith at 225 GHz.

Two 1024-channel acousto-optical spectrometers (AOS) with bandwidths of 50 MHz and 500 MHz were used simultaneously, providing spectral resolutions of 0.025 km/s and 0.25 km/s respectively at 626 GHz. Since the receiver had a double-sideband response, identifying the detected lines required that the local oscillator frequency be shifted, Several molecules (e.g. SO_2, CH_3OH, CS) having transitions near 626 GHz were detected and identified using the JPL Submillimeter Spectral Line Catalog (Pickett et al. 1991), which helped to verify the performance of the system. All the observations were made using a position switching calibration technique. We measured a beam efficiency of about 30% on Jupiter. SPW have used for their map of OMC-1 a beam efficiency of 60%, as measured on the Moon and suitable for extended sources where sidelobes play a role. For Orion A, using a beam efficiency of 45% seems a reasonable compromise between the two limits since the region of the cloud that we observed is a dense clump about the angular size of the beam. For similar reasons, because the main core of Mon R2 is known to be clumpy at the sampling resolution of the 12" beam, it cannot be truly considered an 'extended' source, Hence we have also used a calibration factor of 4570 for its spectra.

3. RESULTS

Table 1 lists the sources which were searched for HCl. We very clearly detected HCl in two clouds, OMC- 1 and Mon R2, and possibly in the circumstellar envelope IRC+10216. We did not detect HCl in W3(OH) at an rms level of 0.83 K, nor in NGC2024 at an rms level of 0.16 K. HC1 was detected toward Orion KL in OMC- 1, the 'hot core' region known to be associated with the IRAS point source IRc2. At this location, we found a very strong line (12 K) and a large velocity dispersion blending the hyperfine components. 'l'he choice for pointing, 60" south of Orion KL, in the so-called 'extended ridge' of OMC- 1, was motivated by a need for clearly separated hyperfine components in order to derive an optical depth, This position corresponds to the 'LS 1' clump seen in CS J=2-1 by Mundy et al (1986) and to a local maxi mum in the recent HC1 J= 1-0 map of SPW.

Table I

Sources Coordinates and $H^{35}Cl$ Detections.

Source	RA (1 950)	DEC (1950)	VLSR (km/s)	T_A^*(K) Central Component
Orion KL	$05^h32^m47.0^s$	-05 °:24':24.0"	**+9.5**	12.1 ± 0.98
Ori A (LS1) [a]	$05^h32^m47.0^s$	-05 °:25':24.0"	**+9.5**	5.6 ± 0.98
Mon R2	$06^h05^m22.0^s$	-06 °:22':25.0"	+10.5	1.1 ± 0. 15
W3(OH)	$02^h23^m16.5^s$	61 °:38':57.0"	**-45.0**	≤ 0.83
NGC 2024	$05^h39^m12.0^s$	-01°:55':42.0"	+10. s	≤ 0.16
IRC+10216	$09^h45^m14.8^s$	13 °:30':41.0"	-26.0	0.6 ± 0.35

[a] **60"** south of Orion KL

Figures 1a, b, and c show the spectra obtained in the 500 MHz AOS for Orion LS 1 and Mon R2. The hyperfine structure of HCl is well resolved and the frequencies are in excellent agreement with theory. One expects the ratio of the components to be 1:3:2 in the optically thin limit, and 1:1:1 in the optically thick one. Saturation is seen in the spectra. Because the velocity

separation of the hyperfine components is larger than their FWHM, the ratio of the three hyperfine intensities can be used to derive the optical depth of the transition. In Fig, lb, the spectrum of $H^{37}Cl$ also shows the hyperfine structure although the magnitude of the F= 1/2-3/2 component is on the order of the rms noise, Table 11 summarizes the peak and integrated intensities derived for the three spectra.

The derivation of the $H^{35}Cl/H^{37}Cl$ ratio requires a careful baseline subtraction that does not remove potential wings and multiple velocity components. Hence, we have used a 'curve of growth' method for finding what we believe were the optimal baselines. For each spectrum, the area of the line as integrated over a velocity interval symmetric about the central frequency, was plotted versus the velocity interval. This curve grows monotonically and reaches a saturation plateau when the line integration is complete. For insufficient (or excessive) baseline subtractions, the plateau has a positive (or negative) slope, and the slope is zero when the best baseline is removed. We defined the end of the plateau at twice the velocity extension of the line, Within the curve of growth for the whole transition, flattening of the curves is also seen every time a hyperfine component has been fully integrated. 'T'his is particularly clear in the Mon R2 data for which the hyperfine components are very clearly defined. Table 11 summarizes our results. In Orion A, the integrated intensity of the individual hyperfine component is underestimated due to the apparent overlap of lines.

Isotopic ratios derived using different techniques are given in Table 111. The ratio of the total integrated intensities underestimates the isotopic ratio if there is saturation in the $H^{35}Cl$ transition, and this saturation is clear from the peak intensities of the individual hyperfine lines. We have also computed the ratio weighted by the, errors. This technique provides smaller error bars since it minimizes the propagation of noise spikes into the ratio, but it also slightly underestimates the ratio of interest.

The total integrated area ratio is $I[H^{35}Cl]/I[H^{37}Cl] = 3.97 \pm 0.35$, and taking into account saturation in the lines (see below), a more plausible ratio is around 4.5- 5. The value derived from

the F=3/2-3/2 integrated area ratio seems too large, and the fact that (his hyperfine component is broader in the $H^{35}Cl$ transition is seemingly the cause of the excess. With $[H^{35}Cl]/[H^{37}Cl]$ ranging from 3.9 to 5, Orion A has a slightly anomalous chlorine isotopic ratio, compared to the *terrestrial* isotopic ratio of -3,

Table II

Measured Peak and Integrated Intensities

(a) Monoceros R2:

Isotope	$H^{35}Cl$
Total Integrated Intensity (K km/s)	5.5 ± 0.2

Line F'-F"	1/2-3/2	'5/2-3/2	312-312
Peak Intensity (K)	0.6 ± 0.3	1.1 ± 0.3	**0.9 ± 0.3**
Integrated Intensity (K km/s)	1.3 ± 0.1	2.3 ± 0.1	**1.9*O.1**

(b) Orion A (KL-60"):

Isotope	$H^{35}Cl$	$H^{37}Cl$
Total Integrated Intensity (K km/s)	30.8 ± 2.2	7.8 ± 0.4

Line F'-F"	1/2-3/2	5/2-3/2	3/2-3/2	1/2-3/2	5/2-3/2	3/2-3/2
Peak Intensity (K)	2.4 ± 0.9	5.5 ± 0.9	4.4 ± 0.9	0,7 ± 0.6	1.4 ± 0.6	1.0 ± 0.6
Integrated Intensity (K km/s)	5.7 ± 1.2	13.1 ± 122	10.7 ± 1.2		3.2 ± 0.2	1.8 ± 0.2

Table III

$H^{35}Cl/H^{37}Cl$ in Orion A (KL-60"): Ratio of Peak and Integrated Intensities

Ratio of Total Integrated Intensities	3.97 ± 0.34		
Line (F'-F")	1/2-3/2	5/2-3/2	3/2-3/2
Ratio of Peak Intensities	> 3.67 ± 3.72	3.84 ± 1.79	4.44 ± 2.93
Error-Weighted Channel/Channel Ratio a	- c	3.14 ± 0.98	4.83 ± 0.30
Ratio of Integrated Intensities b	- c	4.12 ± 0.47	6.28 ± 1.07

a $\frac{\sum_{v1}^{v2}\left(T_A/\sigma^2\right)}{\sum_{v1}^{v2}\left(1/\sigma^2\right)}$

b $\frac{\int_{v1}^{v2} T_{A(35)}.dv}{\int_{v1}^{v2} T_{A(37)}.dv}$

c $H^{37}Cl$ Hyperfine Component within Noise.

4. EXCITATION ANA] YSIS

4.1. *Line Parameter Derivation*

Gaussian fits to the hyperfine structure of the transition provides the optical thickness and the excitation temperature (Kwan and Scoville, 1975; Frerking, Langer and Wilson, 1979). These can then be used as input along with various gas densities and temperatures and species fractional abundances, to a large velocity gradient (LVG) calculations (Goldreich and Kwan, 1974; Leung and Liszt, 1976).

All the spectra have been calibrated by switching the beam on and off the source, so that the measured antenna temperature of each hyperfine line, T_A^*, can be general 1 y expressed by:

$$T_A^* = (B(T_x) - B(T_{dust}) - B(T_{bg}))(1 - e^{-\tau}) \quad (6)$$

where $B(T)$ is the Planck function for a blackbody at temperature T. T_x is the excitation temperature of the transition and τ its optical depth. $T_{bg} = 2.7$ K and T_{dust} is the temperature of the dust. Note that this equation assumes that: 1) the dust is extended, that is, its temperature is the same toward the source and in the OFF position; and 2) it radiates like a perfect blackbody.

The total optical depth τ, the excitation temperature T_x and the FWHM linewidth Δv of the HCl J=1 -0 transition, have been obtained by fitting simultaneously the measured antenna temperatures in the three hyperfine transitions with a simple radiative transfer model which assumes that the number of excited molecules involved in each hyperfine transition F'-F" has a Gaussian velocity distribution. The optical depth can be found from both the ratio of the relative line strengths and the linewidths, while the excitation temperature scales with the absolute line intensities. Table IV gives the derived optical depths and the corresponding column densities for Orion A and Mon R2. We have assumed a negligible dust temperature, and therefore the column densities given here are upper limits. T_x may in fact be smaller if strong background radiation from dust contributes to the excitation of the molecule, but it does not affect the determination of τ, which is independent of T_x.

For the LVG calculations we included the first "/ rotational energy levels and used the collisions] excitation rates of He on HCl recently computed by Neufeld and Green (1994). The hyperfine complexity was addressed by considering that in each J level the populations of the hypcrfine levels are in proportion to their statistical weights. Hence half the molecules populating the J= 1 level are in the F"=5/2 state and the total optical depth of the J= 1-0 transition, τ_{tot} is twice that of the main hyperfine line, τ(F=5/2 - 3/2). Our LVG mode] includes radiation from the cosmic background radiation and from local dust.

Table IV

Gaussian Line Fits: Line Parameters and Derived Properties

Source	Ori A (35)	Ori A (37)	Mon R2 (35)
VLSR (km/s)	9.2	8.8	**10.5**
Av (km/s)	2.4 ± 0.1	2.0 ± 0.1	**0.9- 1,2**
τ_{tot} [a]	2.4 ± 0.2	0.6 ± 0.1	6.0 ± 1.0
T_x (K)	19.0 ± 1.0	16.0 ± 1.0	**10.0 ± ().5**
N (cm^{-2})	4.52 10^{13}	0.69 10^{13}	**1.95** 10^{13}

[a] $\tau_{tot} = 2\,\tau$ (F=5/2-3/2)

4.2. *Orion A*

In the case of Orion A, the linewidth of each hyperfine transition is mainly due to turbulence or infall within the cloud, and therefore the Gaussian approximation for the velocity distribution works reasonably well, with linewidths (FWHM) of -2.4 km/s for $H^{35}Cl$ and -2.0 km/s for $H^{37}Cl$. The difference in linewidth for the two isotopes may be an effect of the difference in the optical depths, $\tau(H^{35}Cl) = 2{,}4 \pm 0.2$ and $\tau(H^{37}Cl) = 0.6 \pm 0.1$. The excess signal between the hyperfine components as well as their asymmetric departure from a purely Gaussian profile may be caused by complex gas motions within the cloud (Walker, Narayanan, and Boss, 1994). We have neglected the possibility of anomalous hyperfine ratios (Gonzalez-Alfonso and Cernicharo, 1993) due to the absorption of red- or blue-shifted hyperfine transitions by molecules populating the adjacent hyperfine levels and on the same line of sight.

The HCl fractional abundance can be derived if the hydrogen column density is known for this region of OMC-1 over an angular size of about 12". A value of $N(H_2) = 3\ 10^{22}$ cm^{-2} was given by BKP (1985), but their observation at an angular resolution of 1' smoothes out regions of very different densities. For the ridge quiescent region, slightly lower values of 3-7 10^{23} cm-2 have been proposed by Liszt et al (1974) and Westbrook et al (1 976), and more recently 2 10^{23} cm^{-2} by

for dust temperatures as low as 15 K. For T_{dust}=17 K, as shown in Fig. 3b, the T_A* and τ_{tot} contours have become parallel, so that there is no solution matching the observations,

Figure **4** shows how the solutions evolve in the density-fractional abundance plane for a variety of dust temperatures, Interestingly, most solutions occur for densities near n(H)= 10^7 cm^{-3}, i.e. the critical density, except when the dust becomes warm enough that it significantly pumps the J= 1 level, as expected. In Fig. 3a, we note a flattening of the optical depth contours around the critical density, indicating the transition between completely collisional excitation and radiative excitation. What the LVG calculations seem to provide is an efficient way to constrain the *dust* temperature from the observations, since depending on T_{dust}, the fractional abundances and hydrogen densities which are solutions can differ by an order of magnitude or more. Some amount of dust radiation seems required to provide the observed X(HCl) - 1.5 10^{-10} for Orion,

In the above estimation of the dust temperature, the dust is considered to be a black body emitter of radiation, Since the actual emissivity of dust gi tins is a complex and unknown function of their physical and chemical properties, we also performed the LVG calculations using a "gray body" model for the radiation by the dust ($B(T_{dust})$ - λ^{-2}). As expected, we find that under the gray body assumption the maximum dust temperature for which a solution can be found is increased. In this case our observations of Orion (and Mon R2, see below) allow warmer dust solutions, typically up to T_{dust}=T_{gas}. Note that assuming a gray body instead of a black body plays little role if the values of τ_{tot} and T_{dust} are small, so that this method for setting a boundary on the dust temperature works better for optically thin lines.

4.3. *Monoceros R2*

IRS 3 in Mon R2 corresponds to a high density clump ($n(H_2)$> 104 cm^{-3}) of the main core, hence capable of collisionally exciting the HCl J= 1-0 transition. However, the observed transition can be excited by a strong radiation field as well. From the hyperfine ratio of the spectrum, we derived a relatively large total optical depth, τ_{tot} = 6.05 1.0, and a FWHM linewidth Av = 1.1

kin/s ± 0.1, in excellent agreement with the value of Av found by Montalban et al. (1990) for the nearby NH_3 clump called 'D', at V_{LSR} = **10.8** km/s. This yields an HCl column density of 4.4 10^{14} cm^{-2}. Assuming $N(H_2)$ = 1,5-3 10^{22} cm^{-2} (Montalban et al., 1990, Gonatas, Palmer, and Novak, 1992), we find $X(HCl)$ -6.5 10^{-10} and a depletion of chlorine by 175. Hence chlorine is less depicted in this region of Mon R2 than in OMC- 1. Figure **5** shows the Mon R2 and OMC- 1 depletion rates plotted as a function of $N(H_2)$, along with the data compiled from other authors, including that toward the diffuse clouds.

For Mon R2, we have performed LVG calculations assuming a gas temperature of 40 K (Montalban et al., 1990, Maddalena et al., 1986) and a velocity gradient of about 4 km/s/pc. This velocity gradient assumes that the depth of the. source is similar to its projected size on the sky, that is, about 0.25 pc considering the 1' size of the associated CS clump. In the black body dust hypothesis, the LVG calculations offer solutions for the observed $\tau_{tot} \simeq 6$ and $T_A^* \approx 1.1$ K only if $T_{dust} < 12$ K (see Fig. 4). If the dust is colder than 10 K, the corresponding gas density and fractional abundance are respectively 5 10^6 cm^{-3} and X(H ^{35}Cl)= 2 10-] ^{1}. Note that these solutions give us very similar conditions of density and HCl fractional abundance for Mon R2 and OMC-1, despite the very different gas temperatures and velocity gradients. The slightly smaller hydrogen densities (for a particular T_{dust}) in the case of Mon R2 can be explained by the fact that collisional excitation is more important at smaller velocity gradients. As for Orion, the sharp boundary between solution and no-solution dust temperatures can be used to set an upper limit on the amount of dust radiation, but this upper limit is relaxed when a dust gray body model is used. Assuming a gray body dust emission, the fractional abundance obtained from the observed column density, $X(H^{35}Cl)$ = 1.6 **10-10,** can be modeled with $T_{dust} \simeq 30$ K and $n(H_2)$ - 10^6 cm^{-3}, implying that moderately warm dust must be present within the source to explain the observations.

In addition to potential errors originating from the calibration of T_A and from the derivation of τ_{tot} from the hyperfine ratio, most uncertainties in the above analysis using the LVG model would come from inexact assumptions made on T_{gas} and on dv/dz. Fortunately, one has enough

knowledge on both parameters for Mon R2 and Orion A that these errors are small and do not qualitatively modify the LVG solutions. (Fig. 4). However, to show the dependence on T_{gas} we have also calculated a case for Mon R2 assuming a lower gas temperature, 30 K rather than 40 K, and find that the fractional abundance of HC1 increases.

5. DISCUSSION

5.1. *Isotopic Ratio*

The chlorine isotopic ratio derived from the total integrated intensities is 4.0 ± 0.3, slightly in excess (x 1.3) of the solar value of ~3. Furthermore, this value is an underestimate due to saturation in the main hyperfine component. The ratio of the fractional abundances derived from the measured optical depths is closer to 5.

Isotopic anomalies found in carbonaceous chondrites are suggestive of an interaction between the protosolar nebula and some nearby supernova (SN) before the solar system was formed. Supernovae ending the life of large mass stars ($M > 10\ M_{\odot}$) play an essential role in scattering heavy elements throughout the interstellar medium. Supernovae eject gas and dust over a volume 50 pc in diameter within 10^5 yr. These chemical diffusion timescales are very short compared to the timescale of the galactic motions (10^8 yr) which stir and wash out chemical non-uniformities. Although SN remnants as large as 50 pc in diameter are difficult to detect, there is now much evidence that SN bubbles can compress interstellar clouds and initiate star formation. The Orion molecular cloud is one example of this process (cf. Bally et al., 1991) and Barnard's loop is one relic of an expanding shell. OMC-1 is near an OB association, characterized by a high SN explosion rate (up to 10-20 times during an association lifetime). Much molecular material has been swept up by SN explosions from the HII region presently surrounding the Trapezium stars.

The elements likely to show evolutionary effects via an isotopic ratio are those for which different isotopes are formed via different mechanisms. For example, unlike ^{29}Si and ^{30}Si, only ^{28}Si can be formed during the explosive carbon burning phase and isotopic anomalies have been

found in the interstellar medium for Si in favor of ^{28}Si (Wannier, 1980). Chlorine should also show evolutionary effects since ^{35}Cl and ^{37}Cl are produced in different processes during the last evolutionary stages of large mass stars. The ^{35}Cl and ^{37}Cl nuclei are produced in the layer whose temperature becomes greater than $3\ 10^{9}$ K, at typical densities of 10^{6} g cm^{-3}, i.e., just before the so-called 'iron group' layer. Within the scenario of explosive oxygen burning, further creation of ^{35}Cl at the temperature of $2.6\ 10^{9}$ K and densities of $2\ 1\ 0^{5}$ g cm^{-3} is possible, within the few seconds that the supernova explosion lasts. Like ^{28}Si for Si, it is ^{35}Cl, that is the chlorine isotope with the smallest atomic number, that is expected to show a production increase. Unfortunately, most models of hydrostatic or explosive nucleosynthesis in type Ia and type II supernovae (e.g. Hashirnoto et al., 1992) do not compute the production of ^{37}Cl, nor its integrated ejects abundance. In order to answer these questions, more observations of the two HC1 isotopes are required, in particular toward c1oucIs having different physical properties and different stellar mass distributions.

5.2. *Depletion of HCl*

Assuming that HCl represents about 30% of the total chlorine nuclei in the gas-phase (SPW, 1994), we find a fractional abundance of about $5{,}0\ 10^{-10}$ for Orion and $2.1\ 10^{-9}$ for Mon R2. Such low abundances yield a very high depletion factor, around '/40 for Orion LS 1 and 175 for Mon R2, considering the chlorine solar system"" fractional abundance of $\mathbf{3.7}\,10^{-7}$ (Anders and Grevesse, 1989). This result confirms the density-depletion correlation already noted by Jenkins (1987) in diffuse clouds, suggesting that the proportion of chlorine nuclei condensed onto dust grains increases with density. Figure 5 shows the chlorine depletion-hydrogen column density correlation, using observations of a variety of diffuse and dense clouds made by several authors.

The observed depletion relative to hydrogen of many atomic species in interstellar clouds correlates with cloud density (Joseph et al, 1986), and several authors have suggested dust-gas interactions via ion-grain collisions as the depletion mechanism (Snow, 1975; Snow and Jenkins, 1980) in diffuse regions. This suggestion is further suppoi ted by another correlation between the

depletion rates and the first ionization potentials (on which the sticking coefficients depend) of the atomic species considered. Depletion in the shielded higher density regions takes place between chlorine atoms and HCl with grains. If the dust is moderately warm (15 K $< T_{dust} <$30 K) only the highly polar HCl can remain on the grain (cf. Bergin, Langer and Goldsmith, 1995)

5.3. *Dust*

The HII region M42 is located in front of OMC- 1, overlapping with it in projection. The characteristics of the dust in the cold and hot regions of OMC-1 have been studied by Bally, Langer, and Liu (1991) who compared the dust far-infrared emission seen by the IRAS satellite with maps of ^{12}CO and ^{13}CO emission. The spatial distribution of cold (25 K) and warm (40-200 K) dust has been investigated by Mezger, Wink and Zylka (1990) who mapped the dust λ1.3-mm emission. They have shown that compact centers of warm (100 K) dust emission coincide with molecular gas condensations detected in ^{13}CO, CS, and H^{2}CO maps, while the cold dust detected at longer wavelengths (> 100 pm) is distributed throughout the molecular clouds. The cold dust throughout OMC- 1 along with the slightly" warmer dust (>40 K) emitting within a thin photodissociation surface layer are mostly heated by the interstellar radiation field originating from the nearb y Trapezium stars. The warm dust emissi on centers associated with the gas condensations of typical solar masses (5-50 MO) and very high density (1 0^{5}-10^{8} cm^{-3}) are. probably self-luminous embedded pre-main sequence stellar objects. They are roughl y distributed along the 12-pc north-south filament of OMC- 1, suggestive of shock-triggered star formation. The CS J=2- 1 clump LS 1 where a peak of HCl emission has been detected is located along this filament, about 60" south of FIR-2 and slightly north of FIR-3. Schilke et al (1994) have pointed out that all the peaks of continuum emission FIR- 1, FIR-2 and FIR-4 found by Mezger, Wink and Zylka (1990) have their counterpart in the HC1 J= 1-0 emission map, with the exception of FIR-3, which is too far south to be associated with this HCl J=1-O peak and LS 1. Therefore the HC1 J=1-0 emission seems to reproduce the lack of correlation exhibited by the CS J=2- 1 emission with regard to the dust FIR emission. Our excitation analysis assuming black body dust emission implies that 5-15 K cold dust

is mixed with the very dense gas. These values seem low for physical temperatures of the dust, especially in a condensation at $n>10^7$ cm^{-3}, where the gas and dust should be thermally coupled. This contradiction may indicate that the continuum radiation from *warmer* dust at 480 μm is not optically thin, or that the dust radiates not as a black body but as a gray body (see section 4.2). Unlike the other gas-dust condensations aligned north-south in OMC- 1, the LS 1 clump is probably a gas condensation, containing no embedded pre-main sequence object, whose dust is heated by the local radiation field and by its interaction with the gas.

In the gas condensation associated with IRS3 in Mon R2, the depletion is smaller than for Orion but still fits the density-depletion correlation discussed above, despite the fact that physical conditions in Mon R2 are quite different from those in OMC- 1, with respect to the gas density, the kinetic temperature, and the dust temperature, Infrared studies have shown high dust column densities in this region (Howard et al, 1995), and Montalban et al. (1990) find extinctions around A_V=21mag. from ^{13}CO measurements. Moreover, *ROSAT* X-ray observations reveal in the denser regions of Mon R2 several young stellar objects undetected at near-infrared or visible wavelengths (Montmerle, 1994), suggestive of much higher extinction (A_V>40 msg.). A very high dust opacity at 480 μm would also be consistent with the low effective dust temperatures required to explain our LVG calculations. Since IRS3 is located at a peak of ^{13}CO and CS(5-4) emission, we expect the density to be larger than 10^6 cm^{-3}. In the nearby 'D' clump, Montalban et al. (1990) find a gas density greater than 2 10^4 cm^{-3} at a kinetic temperature of 30 K. From high resolution maps in both NH_3(1 ,1) and in NH_3(2,2), these authors find that the gas temperature ranges between 25 K and 45 K throughout the whole cloud, except at the position of IRS1, where they determine a kinetic temperature of about 100 K. There, the huge amount of UV radiation (1 0^3 times larger than the average interstellar radiation field) required to provide such a high gas temperature, may release the most volatile elements of grain mantles into the gas phase, creating the apparent increase of the HCl abundance. This scenario of evaporation from recently heated grains has been invoked to explain the large abundance of ammonia seen in regions of large UV field, where NH_3 would otherwise be photodissociated (Gusten and Fiebig, 1988).

6. CONCLUS1ON

The ground-state transition of HCl was detected in Orion A and Monoceros R2 with the CSO using a submillimeter-wave receiver built at JPL to operate around 626 GHz. The hyperfine structure of the HC1 spectra was analyzed to derive the optical depth, and the density and abundance was derived using an excitation analysis with an LVG model which includes radiative pumping from dust emission. The results of the LVG calculations indicate that the observed sources must have very high densities (n> 106-107 cm^{-3}) and low fractional abundances (2 10-11-few 10^{-10}), which imply large depletion factors, Another result is the dependence of the fractional abundances on the dust temperature, and on the dust emissivity (black body vs. gray body law). The HCl fractional abundances of 1.5-610-10 measured in Orion and Mon R2 are higher than the fractional abundance of -210-11 derived from the LVG analysis with no or very cold dust, but are consistent with the values computed when T_{dust} - 15 K (in the black body model), or T_{dust} -50-70 K for Orion A and T_{dust} -40 K for Mon R2 (gray body model). Since the real nature of the dust emission is probably a compromise between these two models, our results suggest that moderately warm dust is needed to produce the observed HCl lines.

Both $H^{35}Cl$ and $H^{37}Cl$ were detected in Orion A, and a $H^{35}Cl/H^{37}Cl$ ratio of 4-5 was derived. Because in dense clouds the chemical path leading from Cl to HCl is fast and with very little branching to other species, this ratio yields a good approximation of the total chlorine isotope $^{35}C1/^{37}Cl$ ratio. The excess relative to the terrestrial isotope ratio of - 3 can be explained by neutron-enrichment occurring during the chlorine-production phase in the large mass stars characteristic of the Orion region,

We are grateful to P, Schilke for sharing data of the HCl J=1-O map of OMC- 1 and to D. A. Neufeld and S. Green for providing their computed HCl collisional excitation rates prior to publication. We also wish to thank T. G. Phillips and W. R. McGrath for their support of the project, S. Gulkis, and T. Spilker for their valuable collaboration during the observations, and H. G. LeDuc and B. Bumble for manufacturing the S1S junctions used in the receiver. This research

was conducted at the Jet Propulsion Laboratory, California Institute of l'ethnology, under contract with the National Aeronautics and Space Administration. The CSO is supported by NSF contract AST 93-13929 to the California Institute of Technology. Morvan Salez has been a Resident Research Associate of the National Research Council.

FIGURE CAPTIONS

FIG. Observed spectra showing hyperfine components (solid line) and Gaussian line fits (dashed line) of (a) $H^{35}Cl$ and (b) $H^{37}Cl$ in Orion A (60" south of 13 N-KL); (c) $H^{35}Cl$ in Monoceros R2.

FIG. 2. Integrated intensity for the a) $H^{35}Cl$ and (b) $H^{37}Cl$ J= 1-0 lines versus the velocity interval from line center ("curve of growth"), after removal of the optimum baseline, The integration extends symmetrically from the transition central frequency. The saturation in both curves around 15-20 km/s indicates when the line is fully integrated, and the *total* integrated intensities used for the ratio of Table III are given by the saturation values (dashed lines). Curve (c) shows the averaged *channel-per-channel* ratio of the two spectra. The minimum reached around 10 km/s results from the larger optical depth of $H^{35}Cl$ weakening $T(H^{35}Cl)/T(H^{37}Cl)$ near the central hyperfine component .

FIG. 3. (a) Antenna temperature T_A^* and optical depth τ_{tot} =2 τ(F=5/2-3/2) of the $H^{35}Cl$ J= 1 -O transition, calculated with the LVG model as a function of the hydrogen density and of the HCl fractional abundance in the Orion A cloud, assuming T_{dust} = 5 K. Only one point in the density-HCl abundance plane, indicated by the arrow, is a solution of the observed values of T_A^* and τ_{tot}; (b) Same as (a) but assuming warmer dust, T_{dust} = 17 K. There is no solution corresponding to the observed T_A^* and τ_{tot}.

FIG. 4. LVG model solutions for the transitions observed in Orion A (filled triangles) and Mon R2 (squares) for different dust temperatures, assuming a black body dust emission. The open square corresponds to T_{dust} = 10 K in Mon R2, using T_{gas} = 30 K.

FIG. 5. Chlorine depletion versus the hydrogen column density, derived from UV absorption measurements in diffuse clouds (Harris, Gry, and Bromage,1986, filled circles; Joseph et al., 1984, empty circles; Federman et al., 1995, cross) or using the HCl J=1 -O transition in dense clouds such as Sgr B2 (Zmuidzinas et al., 1995, empty triangle),

Orion A (BKP, 1986, filled triangle; SPW, 1995, empty square our measurement, filled square), Mon R2 (our measurement, star).

REFERENCES

Anders, E., and Grevesse, N., 1989, Geochim.Cosmochim. Acts 53, 197.

Barlow, M. J. and Silk, J. 1977, ApJ. (Letters), 211, L83.

Bally, J., Langer, W. D., and Liu W., 1991, ApJ., 383, 645.

Bally, J. and Lada, C. J., 1983, ApJ, 265, 824.

Bally, J., Langer, W. D., Wilson, W., Stark, A, A., and Pound, M. W. 1991, Proceedings of IAU No. 147, *Fragmentation of Molecular Clouds and Star Formation*, Ed. E. Falgarone, F. Boulanger, and G. Duvert (Kluwer Academic Publishers, Dordrecht).

Batrla, W., Wilson, T. L., Bastien, P., and Ruf, K., 1983, A&A 128, 129.

Bergin, E. A., Langer, W. D., and Goldsmith, P. F., 1995, ApJ., 441, 222.

Blake, G. A., Keene, J., and Phillips, T. G. 1985, ApJ., 295, 501.

Blake, G. A., Anicich, V. G. and Huntress, W. T., Jr. 1986, ApJ., 300, 415.

Casanova, S., Montrnerle, T., and Andre, P., 1995, ApJ., 439, 752.

Chini, R., Kreysa, E., Mezger, P. G., Gemund, H-P., 1984, A&A 137, 117.

Dalgarno, A., de Jong, T., Oppenheimer, M., and Black, J. H. 1974, ApJ., 192, L37.

Dowries, D., Winnberg, A., Goss, W. M., and Johansson, L. E. B., 1975, A&A, 44, 243.

Federman, S. R., Cardelli, J. A., van Dischoeck, E. F., Lambert, D. L., and Black, J. H., ApJ., 445, 325.

Goldreich, P. and Kwan, J., 1974, ApJ., 189, 441'.

Goldsmith, P. F. and Langer, W. D., 1978, ApJ., 222, 881.

Gonatas, C. P., Palmer, P. and Novak, G., 1992, ApJ., 398, 118.

Gonzalez-Alfonso, E., and Cernicharo, J., 1993, A&A, ?79, 506.

Gusten, S., Chapman, S., 1988, A&A, 204, 253.

Harris, A. W., Gry, C. and Bromage, G. E. 1984, ApJ., 284, 157.

Hashimoto, M., Nomoto, K., Tsujimoto, 'I'., and Thielemann, F.-K. 1992, "Nuclei in Cosmos", *Proceedings of the 2nd international. Symp. on Nuclear Astrophysics,* Karlsruhe, Germany, 6-10 July 1992.

Henning, Th., Chini, R., Pfau, W., 1992, A&A 263, 285.

Heyer, M. H., Snell, R. L., Goldsmith, P. F., Strom, S. E., & Strom, K. M., 1986, ApJ. 308, 134.

Howard, E.M., Pipher, J. L., Forrest, W. J., 1994, ApJ. 425, 707.

Joseph, C. J., Snow, T. P., Jr., Scab, C. G., Crutcher, R. M. 1986, ApJ., 309, 771

Jura, M. 1974, ApJ., 190, L33.

Koresko. C. D., Beckwith, S., Ghez, A. M., Matthews, K., Herbst, T. M., Smith, D. A., 1993, A&A 105, 1481.

Langer, W. D., Graedel, T.E., Frerking, M. A., and Armentrout, P. B., 1984, Ap. J., 277, 581.

Leung, C. M. and Liszt, H. S., 1976, ApJ., 208, 732,.

Liszt , H. S., Wilson, R. W., Penzias, A. A., Jefferts, K. B., Wannier, P. G., and Solomon, P. M., 1974, ApJ., 190, 557.

Maddalena, R. J., Morris, M., Moscowitz, J., Thaddeus, P., 1986, ApJ. 303, 375.

Massi, M., Felli, M., and Simon, M., 1985, A&A, 152, 387.

Meyers-Rice, B. A., Lada, C. J., 1991, ApJ., 368, 445.

Mezger, P. E., Wink, J. E., and Zylka, R., 1990, A&A 228, 95.

Migenes, V., Johnston, K, J., Pauls, T. A., Wilson, T. 1., 1989, ApJ. 347, 294.

Montalban, J., Bachiller, R., Martin-Pintado, J., Tafalla, M., and Gomez-Gonzales, J., 1990, A&A 233,527.

Montmerle, Th., 1994, private communication.

Moore, E. L., Langer, W. D., Huguenin, G. R., 1986, ApJ. 306, 682,

Mundy, L. F., Scoville, N, Z., Baath, L. B., Masson, C. R., & Woody, D. P., 1986, ApJ., 304, L51.

Neufeld, D. A., Green, S., 1994, ApJ., 432, 158.

Pickett, H. H., Poynter, R. L., and Cohen, E. A., 1991, *Submillimeter, Millimeter and Microwave Spectral Line Catalog,* JPL Publication 80-23, Rev. 3,

Smith, D. and Adams, N. G., 1985, ApJ., 298, 827.

Schilke, P., Wahnsley, C. M., Pineau des Fôrets, G., Roueff, E., Flower, D. R., Guilloteau, S., 1992, A&A 256, 595.

Schilke, P., Phillips, T. G., and Wang, N., 1995, ApJ., 441, 334.

Sellgren, K., Smith, R. G., Brooke, T. Y., 1994, ApJ. 433, 179.

Snow, T. P., Jr. 1975, ApJ., 202, L87.

Snow, T. P., Jr. and Jenkins, E. B. 1980, ApJ., 241, 161,

Snow, T. P., 1984, ApJ. 287, 238.

Tafalla, M., Bachiller, R., Wright, M. C. H., 1994, ApJ. 432, L127.

Walker, C. K., Adams, F. C., and Lada, C. J., 1990, ApJ., 349, 515.

Walker, C. K., Narayanan, G., and Boss, A. P., 1994, ApJ., 431, 767.

Walmsley, C. M., and Wilson, T. L., 1985, in *Nearby Molecular Clouds,* European Regional Symp. of the IAU, Toulouse, **1984,** Springer, Berlin Heidelberg Ncw York.

Wannier, P. G., 1980, Ann. Rev, A&A, 18, 399.

Westbrook et al, 1976, ApJ., 209, 94.

Wolf, G. A., Lada, C. J., and Bally, J., 1990, A. J. 100, 1892.

Xie, T. and Goldsmith, P. F., 1994, ApJ., 430, 252,

Zmuidzinas, J., Blake, G. A., Carlstrom, J., Keene, J., and Miller, D.. 1995, ApJ. Letters, 447, L125.

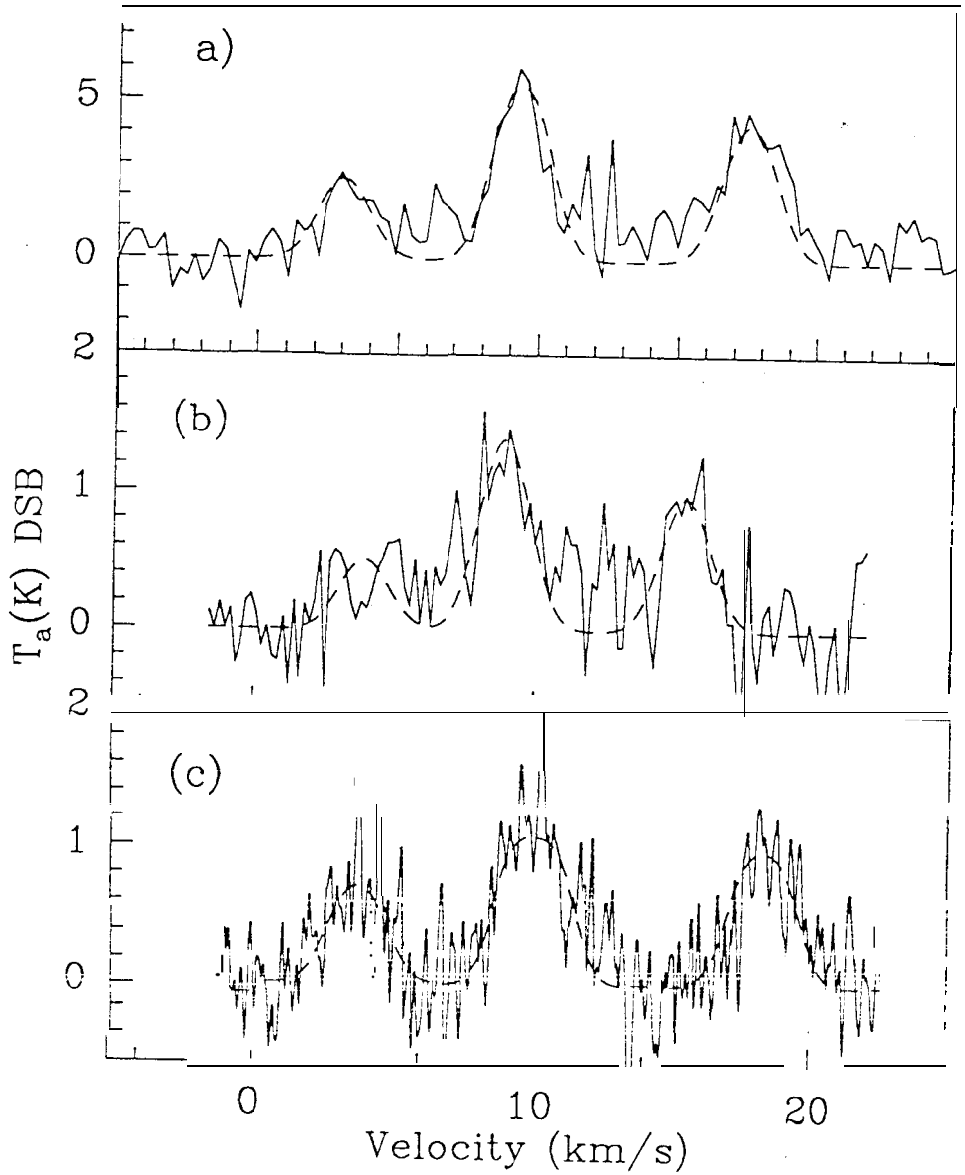
a)
(b)
(c)
5
0
2
1
0
2
1
0
T_a(K) DSB
0
10
20
Velocity (km/s)

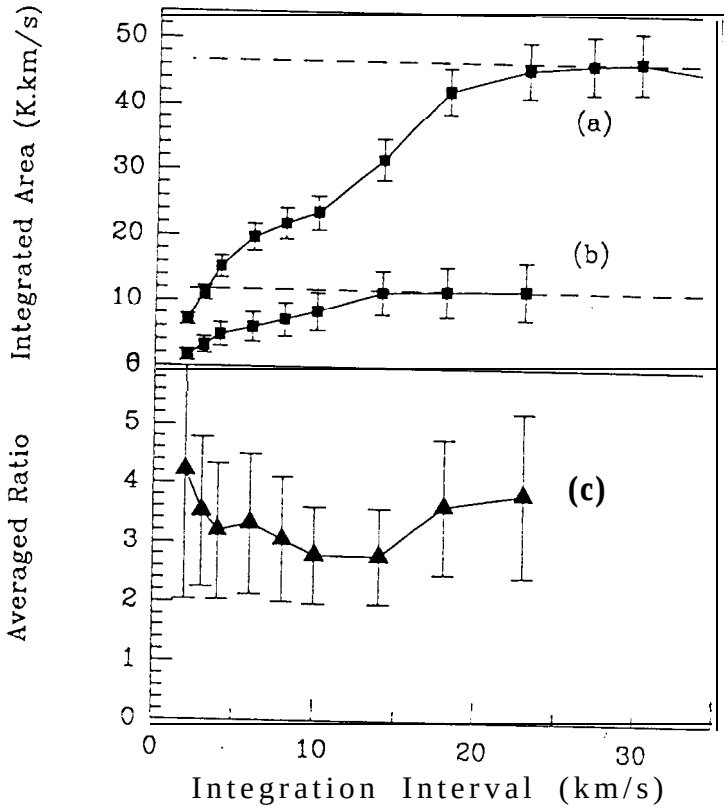
Integrated Area (K.km/s)
Averaged Ratio
50
40
30
20
10
0
(a)
(b)
5
4
3
2
1
0
(c)
0
10
20
30
Integration Interval (km/s)

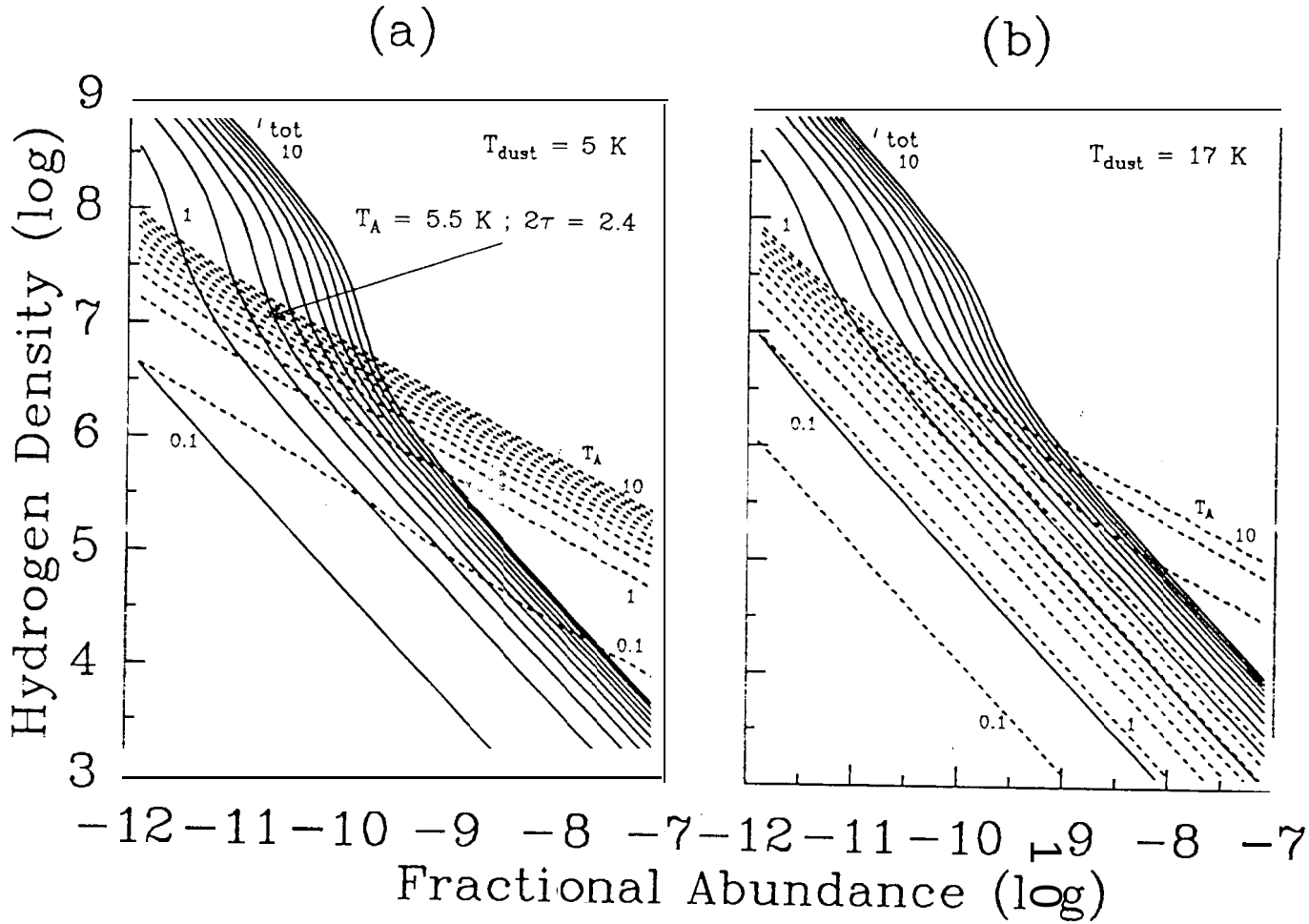
(a)
(b)
Hydrogen Density (log)
9
8
7
6
5
4
3
T_{dust} = 5 K
T_{dust} = 17 K
T_A = 5.5 K ; 2τ = 2.4
tot
10
1
0.1
T_A
−12 −11 −10 −9 −8 −7 −12 −11 −10 −9 −8 −7
Fractional Abundance (log)

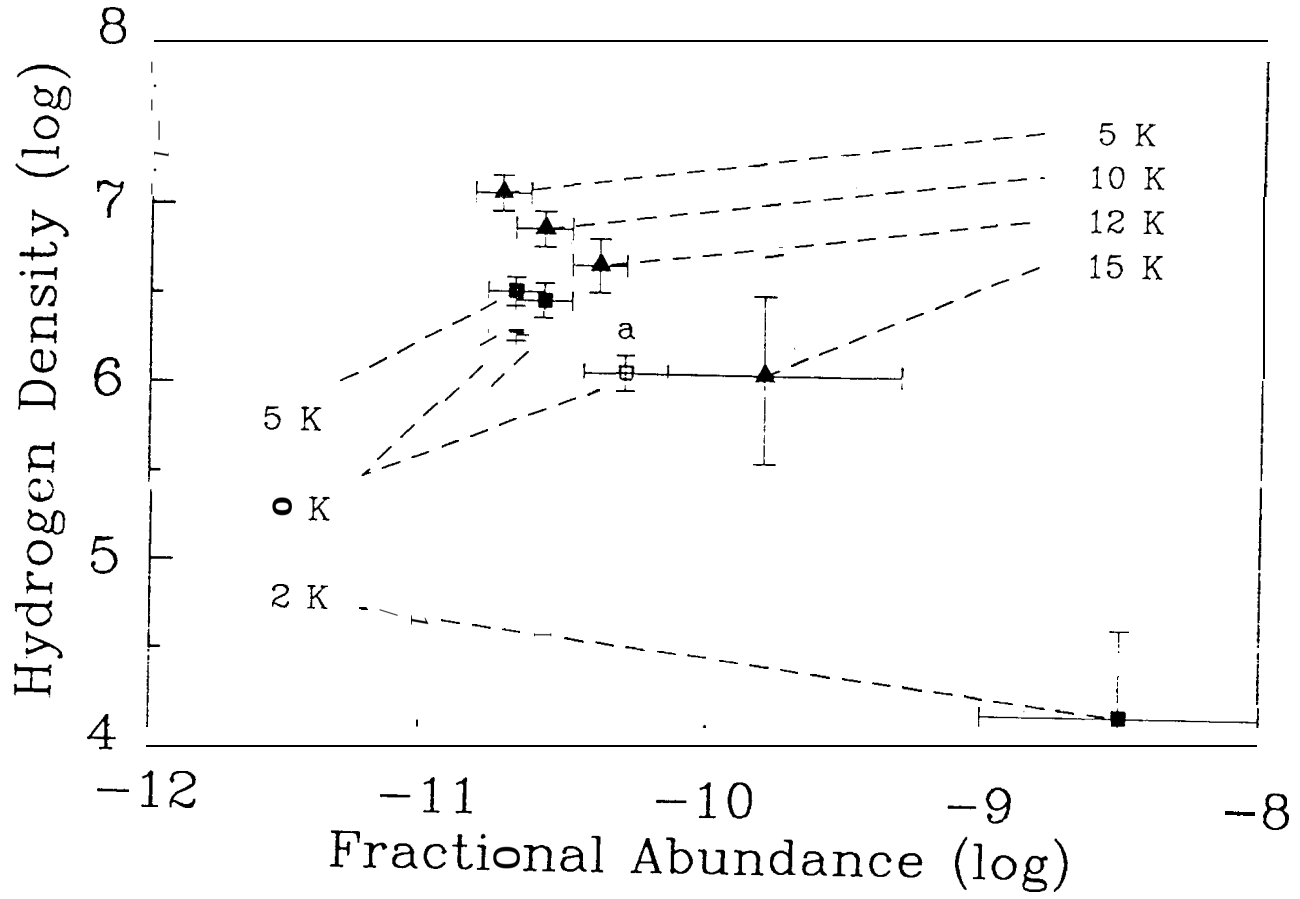
Hydrogen Density (log)
8
7
6
5
4
−12
−11
−10
−9
−8
Fractional Abundance (log)
5 K
10 K
12 K
15 K
a
5 K
0 K
2 K

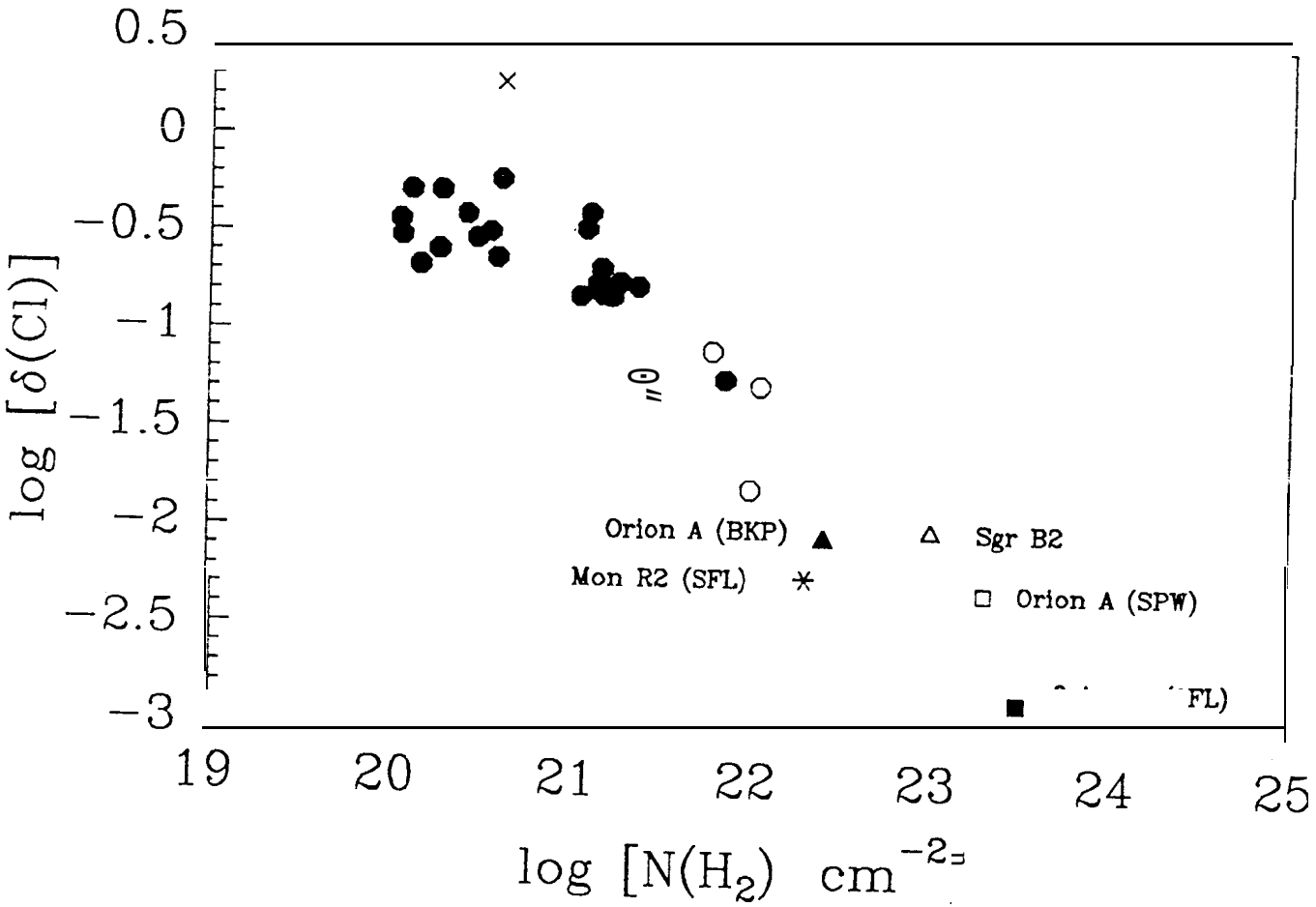
0.5
0
−0.5
−1
−1.5
−2
−2.5
−3
log [δ(Cl)]
19
20
21
22
23
24
25
log [N(H2) cm−2]
Orion A (BKP)
Mon R2 (SFL)
Sgr B2
Orion A (SPW)
FL)